metals

MDPI

Article

The Influence of Spheroidizing Annealing Process on the Microstructure and Low-Temperature Impact Toughness of Q235 Steel Used in Coal Explosion-Proof Equipment

Hongkui Zhang [1,2,3,*], Yipeng Lan [1], Xinming Liu [4] and Guanglong Li [4]

[1] Department of Electrical Engineering, Shenyang University of Technology, Shenyang 110178, China; lanyipengg@163.com
[2] CCTEG Shenyang Research Institute, Fushun 110178, China
[3] Fushun CCTEG Inspection Center Co., Ltd., Fushun 110178, China
[4] School of Materials Science and Engineering, Shenyang University of Technology, Shenyang 110870, China; 15040956021@163.com (X.L.); liguanglong1990@163.com (G.L.)
* Correspondence: 18940021505@126.com

Abstract

To improve the low-temperature impact toughness of Q235B steel, this paper adopts a heat treatment method combining quenching and spheroidizing annealing to enhance its microstructure and properties and conducts a detailed analysis of the evolution of the microstructure of Q235 steel under the spheroidizing annealing process. The results show that spheroidizing annealing at 700 °C has a significant spheroidizing effect on the pearlite structure: after 6 h of annealing, the room-temperature tensile strength reaches 522 MPa, the elongation is 31.28%, and the impact energy is 323.14 J; as the impact temperature decreases, the impact toughness of Q235B steel decreases, but the impact energy can still remain at 291.62 J under service conditions of −20 °C. This is attributed to the spherical cementite formed by spheroidizing annealing, which has better dispersibility and can reduce stress concentration, thereby improving the low-temperature impact toughness.

Keywords: Q235B steel; spheroidizing annealing; mechanical properties; impact toughness; fracture morphology

check for updates

Received: 26 June 2025
Revised: 21 July 2025
Accepted: 22 July 2025
Published: 25 July 2025

Citation: Zhang, H.; Lan, Y.; Liu, X.; Li, G. The Influence of Spheroidizing Annealing Process on the Microstructure and Low-Temperature Impact Toughness of Q235 Steel Used in Coal Explosion-Proof Equipment. *Metals* **2025**, *15*, 833. https://doi.org/10.3390/met15080833

Copyright: © 2025 by the authors. Licensee MDPI, Basel, Switzerland. This article is an open access article distributed under the terms and conditions of the Creative Commons Attribution (CC BY) license (https://creativecommons.org/licenses/by/4.0/).

1. Introduction

Mineral resources are the cornerstone of modern industrial development, providing necessary raw materials for global construction, such as metals, energy, and non-metallic minerals [1–3]. Explosion-proof doors [4], explosion-proof switches [5], explosion-proof conveyors [6], and other commonly used tools for mining resources typically require consideration of material hardness, wear resistance, impact resistance, and corrosion resistance in their design to ensure long-term stable operation in harsh working environments [7,8]. In addition, Q235B steel not only meets the mechanical load-bearing requirements of most components of mining equipment but also has low cost [9–11]. Therefore, in the fields of engineering structures and construction, Q235B steel is highly valued for its excellent strength, elongation, toughness, and formability, as well as its outstanding performance under various environmental conditions [12,13].

As is well known, alloying methods can improve the microstructure of alloy steel, thereby enhancing its strength and enabling it to withstand greater working loads and meet stricter working conditions [14]. Wang et al. [15] found that compared to steel without

added Cr/N, the yield strength of Cr/N alloy steel increased by about 53%, but the impact toughness (CVN) decreased by about 35%. In theory, the CVN of 24Mn-6.3Cr-0.2N steel should be the highest. However, Dastur et al. [16] and Saeed et al. [17] found that in TWIP steel, the reorientation of Mn-C SRO composites leads to higher stress, which in turn reactivates dislocation slip and enhances CVN. It is worth noting that adding elements can lead to the formation of second phases or compounds in the material, and the distribution and morphology of phases or compounds can also affect the mechanical properties of the material. Heat treatment is a more industrialized method of material improvement that can enhance material properties by altering the microstructure of the material without changing its chemical composition.

Therefore, in recent years, more and more scholars have tended to use heat treatment processes to improve the microstructure and properties of various steels. Yu et al. [18] systematically organized the existing experimental data of hot-rolled steel and cold-formed steel after heat treatment. We conducted in-depth research on the influence mechanism of heat treatment on the microstructure of steel structures. And two series of models for residual stress after steel heat treatment were calibrated, improving the accuracy and reliability of the models and providing a valuable reference for researchers in related fields.

Qiu et al. [19] studied the mechanical properties of hot stamping Q235 steel ball shells that were water-cooled at high temperatures and not flattened and found that hot stamping treatment can improve the mechanical properties of Q235 steel to a certain extent. The exposure temperature and water cooling method have limited effects on the elastic modulus of Q235 steel for hot stamping spherical shells but significantly affect the elongation at break, yield strength, and ultimate strength.

Gurumurthy et al. [20] studied the effect of the heat treatment process on AISI 4340 steel. The process first heats the steel to the critical temperature, then places it in a salt bath for 0.5 h, and finally cools it to room temperature in air. The results showed that after isothermal quenching treatment, the microstructure of AISI 4340 steel transformed into ferrite and martensite with high toughness and optimal hardness.

Htun et al. [21] studied the properties of spring steel through quenching and tempering. After quenching, unstable austenite was formed in the microstructure of the spring steel, which was completely eliminated by tempering treatment. After performance testing, it was found that its hardness and tensile strength were significantly improved.

Kini et al. [22] found that the size of annealed microstructure (coarse pearlite) is coarser than that of standard parts, and the chemical composition and microstructure are more uniform. Quenching shows a flat noodle martensite structure, which effectively improves the elongation of AISI 1015-EN 9 steel. Therefore, annealing treatment helps to improve the toughness of steel.

Hwang et al. [23] performed spheroidization treatment on SAE 52100 bearing steel with different initial microstructures, and the results showed that spheroidization annealing of martensitic microstructure can significantly improve the uniformity of the product and reduce its hardness. Wu et al. [24] controlled the spheroidization microstructure by optimizing the spheroidization annealing parameters, which improved the wear and contact fatigue performance of the material. Dutta et al. [25] studied the relationship between the microstructure fraction and ability changes of low-carbon steel during the annealing process through recrystallization kinetics combined with EBSD (electron backscatter diffraction) analysis. Therefore, spheroidization annealing treatment can refine the structure, improve mechanical properties, and enhance material toughness.

Xu et al. [26] found that ultrasonic surface rolling treatment (USRP) of FH36 marine steel improved with grain refinement and increased compressive residual stress but had a poor effect on improving low-temperature impact toughness. Du et al. [27] found that

manganese steel in bcc fcc biphasic structure exhibits high impact toughness due to high residual austenite stability and low martensitic dislocation density. Gumuslu et al. [28] found that austenitic stainless steel can provide good wear protection by forming S-phase through low-temperature nitriding. Matthew et al. [29] reported that after thinning (QL) heat treatment, the volume fraction and lattice parameters of residual austenite in alloy steel increased, and the austenite phase became more similar to a thin film structure. The optimization treatment of the membrane-like austenite phase can further improve the impact toughness of low-temperature low-alloy steel without increasing the content of alloying elements.

From the above content, it can be summarized that the basis for improving the low-temperature impact toughness of materials is mainly through improving the microstructure, reducing internal stress, optimizing phase structure, and reducing dislocation density [22–25], and spheroidization annealing treatment can precisely improve the microstructure and residual stress [19–21]. In order to enhance the performance of Q235B steel components in low-temperature environments, this study conducted heat treatment strengthening on Q235B steel through quenching and spheroidization annealing. The influence of different spheroidization treatment insulation times on the microstructure and properties of Q235B steel was analyzed through microstructure observation and tensile and impact performance testing. This study will lay a theoretical foundation for the application of Q235B steel components in low-temperature environments.

2. Experimental Details

2.1. Experimental Materials

Q235 steel is widely used in the construction field (such as beams, columns), machinery manufacturing field (such as brackets, gears), and mining equipment field (such as explosion-proof doors, conveyors). In the mining industry, it is highly valued for its ability to withstand static and dynamic loads in harsh environments.

Equivalent steels in other regions include the following:

United States: A36 carbon structural steel (ASTM A36), which has similar tensile strength (400–550 MPa) and application scenarios and is often used in bridges and building structures.

Europe: S235JR (EN 10025) [30], with comparable carbon content (approximately 0.20 wt.%) and mechanical properties, is widely used in construction and general engineering fields.

The chemical composition of the Q235B steel used in this study—purchased from an external supplier—is presented in Table 1, with the values being actual measured results. A 4% nital solution was used as the etchant for metallographic structure observation.

Table 1. Chemical composition of Q235B steel.

Elements	C	Mn	Si	S	P	Impurity	Fe
Content [wt.%]	0.12	0.51	0.27	≤0.045	≤0.045	≤0.01	Bal.

2.2. Experimental Method

In this experiment, a muffle furnace was employed to subject Q235B steel to quenching + spheroidizing annealing heat treatment, and the heat treatment process is depicted in Figure 1. According to the equations of Trzaska [31] and Park [32], the temperatures of atomic absorption spectroscopy are estimated to be approximately 726 °C and 865 °C, respectively. A1 is determined to be approximately 726 °C, and A3 is determined to be

approximately 865 °C. First, the specimens were held at a temperature of 1000 °C for 0.5 h, then quenched in a 10% NaCl solution. In this experiment, the research team selected the initial fully annealed and quenched steel microstructure as the starting point for the spheroidization heat treatment study. The spheroidization heat treatment was conducted at 700 °C for durations of 1 h, 3 h, 9 h, and 24 h to observe the effect of different holding times on microstructure evolution. All experimental groups underwent the spheroidization process under a constant temperature of 700 °C. Finally, after the preliminary experiments were completed, the final test parameters were set to heating to 700 °C and holding for 0 h, 3 h, 6 h, or 9 h, followed by air cooling to room temperature, resulting in spheroidized annealed specimens.

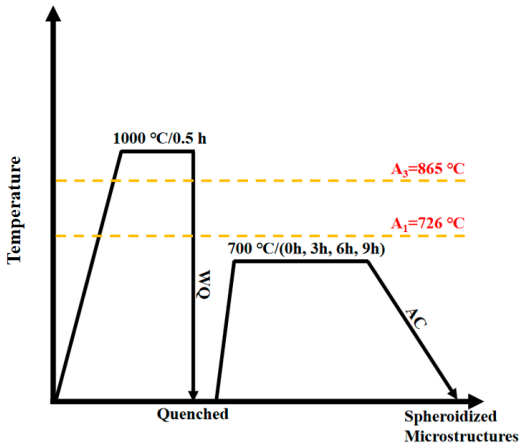

Figure 1. Schematic diagram of quenching + spheroidizing annealing heat treatment process.

2.3. Performance Testing

The microstructure of the specimens was characterized using a laser confocal microscope (OLS4100, Olympus, Tokyo, Japan) and a scanning electron microscope (SEM TM3030, Hitachi, Tokyo, Japan). The tensile strength of the specimens was tested using a universal testing machine (MTS E45, MTS Systems Corporation, Eden Prairie, MN, USA) at a tensile speed of 1 mm/min, and the size of the tensile specimens is shown in Figure 2. Three sets of tests were conducted for each specimen. The impact toughness of the specimens at different temperatures was tested using an oscillating impact tester (MTS ZCJ100, MTS Systems Corporation, Eden Prairie, MN, USA), and the size of the impact specimens is shown in Figure 3. The type of Charpy pendulum is the Charpy V-notch pendulum, with a V-notch depth of 2 mm. The impact tests were conducted at 20 °C, 0 °C, −20 °C, and −40 °C, with three replicate trials performed at each temperature. Finally, the tensile and impact fracture morphologies of the specimens were observed and analyzed using a scanning electron microscope (GeminiSEM300, Carl Zeiss AG, Oberkochen, Germany).

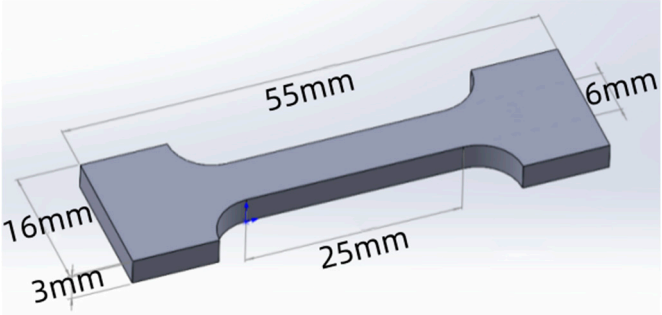

Figure 2. Tensile specimen size.

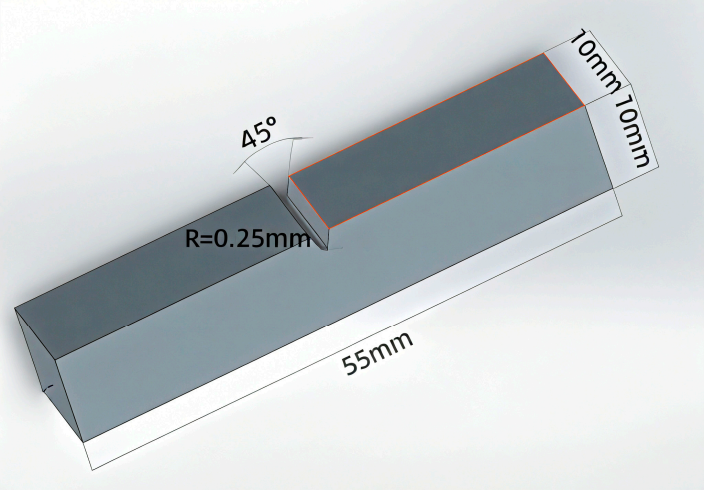

Figure 3. Impact specimen size.

3. Results and Discussion

3.1. Spheroidizing Annealing for Treatment and Microstructure Evolution

The microstructure of Q235B steel at different holding times during spheroidization annealing is shown in Figure 4. As anticipated, the fully annealed specimens (denoted as 0 h) exhibited the characteristic layered pearlite microstructure [33]. Inside the pearlite, carbides are distributed in a layered form, and at a spheroidization time of 3 h (Figure 4b), the lamellar carbides show a tendency to gradually fracture, without observing the diffusion of carbides. When the spheroidization time increased to 6 h (Figure 4c), spheroidized carbide particles began to appear in the microstructure of the pearlite, and the distribution of spherical carbides in the pearlite showed a relatively uniform state. As the spheroidization time was further extended to 9 h, as shown in Figure 4d, the shape of the spherical carbides remained basically unchanged. However, during the long-term high-temperature insulation process, the microstructure of the matrix showed an over-insulation phenomenon. The ferrite tissue undergoes growth [34].

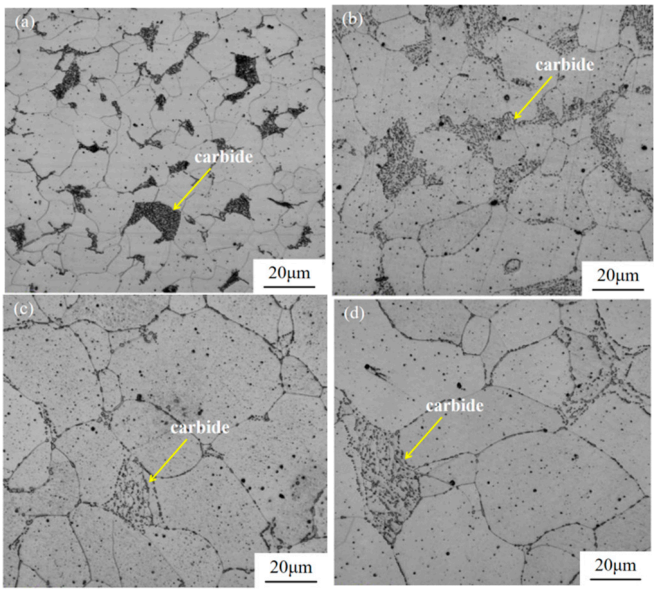

Figure 4. LSCM images of the microstructure of Q235B steel substrate at different holding times: (**a**) annealed specimens; (**b**) spheroidization time of 3 h; (**c**) spheroidization time of 6 h; (**d**) spheroidization time of 9 h.

Figure 5 elaborates on the evolution of the matrix structure of Q235B steel during the spheroidizing annealing process. Ferrite appears as large chunks, with relatively large grains; conversely, pearlite manifests as spherical and blocky shapes with smaller grains and a banded microstructure. By comparing the matrix structures of Q235B steel under different spheroidizing holding times, it can be observed that the matrix after spheroidizing annealing consists of ferrite and pearlite, and the carbides in pearlite present a lamellar structure. This is because after quenching treatment, austenite in Q235B steel transforms into martensite [35], and the quenched steel is reheated to 700 °C and immediately (fully annealed specimens) air-cooled to room temperature. At this time, the recovery and recrystallization changes in ferrite in the matrix are not complete, and the carbides cannot be completely spheroidized, resulting in the internal carbon atoms not reaching the expected spheroidized state, as shown in Figure 5a. In this case, due to the suitable temperature, the diffusion rate and solubility of carbon are both high, which is conducive to the spheroidization process; however, in complete annealing treatments, if the annealing time is insufficient, some layered pearlite may not have fully decomposed or only just decomposed into spherical carbides, resulting in the coarsening of certain carbides. In addition, it can be observed that there is non-uniformity in the layered boundaries inside the pearlite, accompanied by the initial appearance of the melting phenomenon. When different spheroidizing holding times are applied, the matrix structures are as shown in Figure 5b–d. The lamellar carbides within pearlite begin to decompose, forming initial spherical carbides, and some larger lamellar carbides begin to split into multiple smaller spherical carbides [36–38]. Compared with the specimens prepared without holding (Figure 5a), the spheroidization degree of carbides significantly increases during the holding process, and the matrix structure becomes more uniform. This is because during the holding period, the dislocation, defects, and subgrain boundaries at the edges of cementite with a small surface curvature radius undergo a fusing process first, resulting in a higher carbon concentration in the balanced α-Fe. The diffusion of carbon reduces the carbon concentration in α-Fe at the locations with a small surface curvature radius, thereby dissolving the cementite; in planar α-Fe, the carbon concentration increases, precipitating new cementite [39]. Through the diffusion of carbon in α-Fe, the carbon in the small carbide particles is absorbed by the growing particles and gradually spheroidized. These two processes jointly complete the morphological transformation from lamellar to spherical cementite. With the holding time reaching 6 h, the lamellar carbides have completely transformed into spherical carbides, achieving a relatively high spheroidization degree, and the spherical carbides gradually distribute evenly in the ferrite matrix, as shown in Figure 5c [40]. As the holding time reaches 9 h (Figure 5d), the atoms dissolved in the solid solution have more time to diffuse to the grain boundaries, resulting in grain boundary movement and grain merging and growth, and the microstructure becomes coarse.

As depicted in Figure 6, the XRD spectra of Q235B steel with different holding times during spheroidizing annealing are presented. Clearly, only ferrite peaks and carbide peaks exist in the matrix, indicating that the matrix consists of these two phases. In the initial state, the XRD pattern displays distinct characteristic diffraction peaks of carbides. As the spheroidizing annealing process progresses, some lamellar carbides begin to spheroidize, leading to a certain degree of weakening in the intensity of the characteristic diffraction peaks of carbides. At this stage, the carbides are no longer sufficiently distinct to appear clearly in the XRD pattern, while the broadening of the ferrite characteristic peaks suggests either ferrite grain growth or strain accumulation at grain boundaries [41].

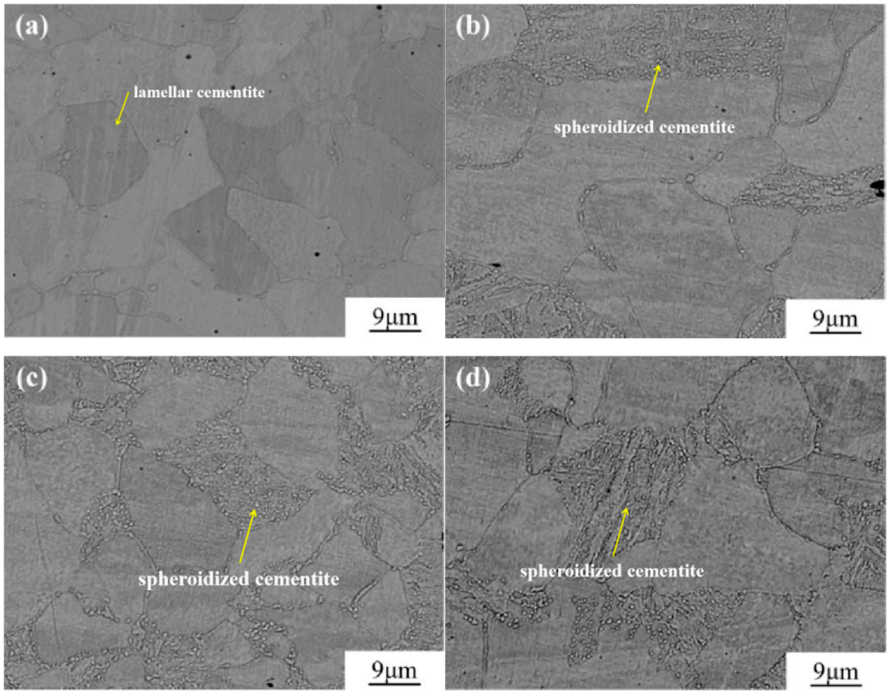

Figure 5. SEM images of the microstructure of Q235B steel substrate at different holding times: (**a**) annealed specimens; (**b**) spheroidization time of 3 h; (**c**) spheroidization time of 6 h; (**d**) spheroidization time of 9 h.

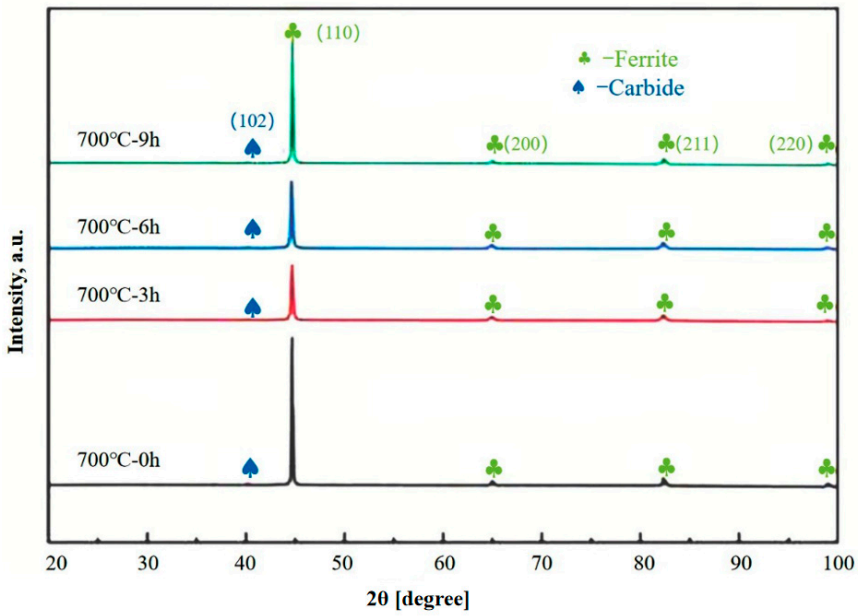

Figure 6. XRD patterns of Q235B steel at different holding times.

3.2. Spheroidizing Annealing for the Treatment of Mechanical Properties

The tensile properties of the specimens were tested using a universal testing machine (UTM5105), Q235B steel specimens with different holding times in the spheroidizing annealing treatment were selected, and their tensile specimens are shown in Figure 7 and Table 2. As shown in Figure 7, extending the holding time can significantly improve the tensile strength and elongation of the material.

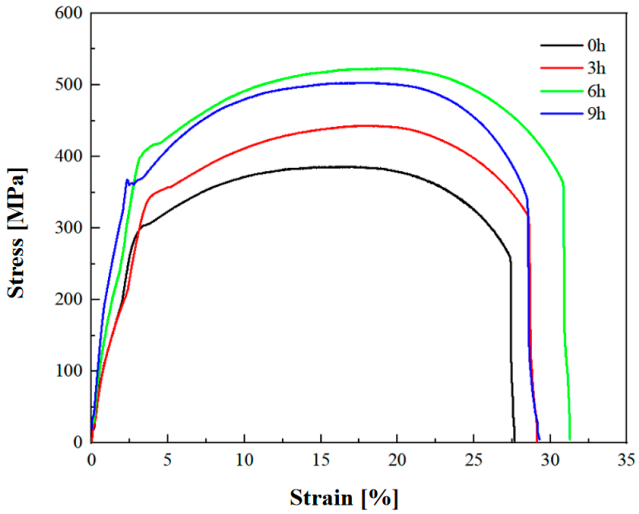

Figure 7. Tensile stress–strain curves of Q235B steel with different heat treatment processes.

Table 2. Yield strength and ultimate tensile strength of Q235B steel under different heat treatment processes.

Spheroidization Annealing Time [h]	Yield Strength [MPa]	Ultimate Tensile Strength [MPa]
0	292.21	385.63
3	329.86	439.81
6	392.08	522.77
9	353.42	503.71

For the specimen with fully annealing holding, the tensile strength is 385.63 MPa, and the elongation is 27.66%. After 3 h of spheroidizing annealing holding, the tensile strength of the specimen is 439.81 MPa, and the elongation is 29.13%, which has increased by 14.02% and 5.31%, respectively. After 6 h of spheroidizing annealing holding, the tensile strength of the specimen is the highest, reaching 522.77 MPa, and the elongation is 31.28%, which has been increased by 35.58% and 13.08%, respectively. After 9 h of spheroidizing annealing holding, the tensile strength of the specimen slightly decreases to 503.71 MPa, while the elongation is 29.27%. However, compared with the specimen without holding treatment, its tensile strength and elongation have increased by 30.64% and 5.82%, respectively.

According to the comparison with the American standard A36 carbon structural steel, the tensile strength range of Q235B steel after spheroidizing annealing treatment is 400 MPa to 550 MPa, and the performance has met the national requirements for the same grade steel [42].

The strengthening mechanism of spheroidization annealing on tensile strength is discussed as follows. The interaction between dislocations and spheroidized carbides is the reason for dynamic strain aging (DSA); when lamellar carbides transform into spheroidal carbides, stacking faults and dislocations often require higher stress to fracture from the spheroidized carbide region [43]. Quenching treatment enables the steel to provide greater tensile strength when subjected to force, thereby enhancing the bearing capacity of the material. In order to further improve the toughness of Q235B steel, 700 °C spheroidizing heat treatment was carried out to promote the diffusion of carbon atoms. During the tensile process, carbon atoms gather below the dislocation line to form a Cottrell atmosphere, which forms a pinning effect on the dislocation line, thereby improving the yield strength of the steel [44].

The MTS ZCJ100 oscillation impact testing machine was used to conduct room temperature impact toughness tests on specimens that had undergone 6 h spheroidization and annealing treatment. The results were compared with the received matrix specimen, and a displacement absorption energy curve was plotted, as shown in Figure 8. The room temperature impact energy of the matrix specimen is 24.26 J, and the fracture mechanism is cleavage fracture, with the specimen breaking; the room temperature impact energy of the spheroidized annealed specimen is 360.52 J, and the fracture mechanism is that the material undergoes plastic deformation, resulting in microporous aggregation fracture. The macroscopic manifestation is bending only due to the impact of the pendulum, tearing at the starting point, and overall, not breaking. This means an average growth of 1386.07%, significantly exceeding expectations. By contrast, as a benchmark, A36 carbon structural steel typically requires a minimum impact energy of 27 J at standard temperatures (typically room temperature, 70 °F). The average impact energy of Q235B steel after spheroidization and annealing treatment is 360.52 J, and its performance greatly exceeds the national standard of similar steels [42].

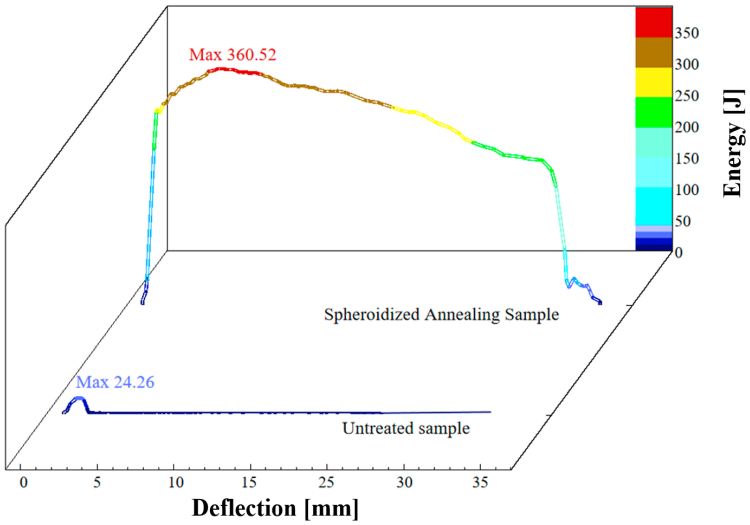

Figure 8. Displacement absorption energy curves of spheroidized and untreated specimens.

The microstructure obtained from the fully annealed specimen has a spherical cementite ferrite banded microstructure, inheriting the original pearlite ferrite microstructure. For the specimens corresponding to 0, 3, 6, and 9 h of spheroidization time, it can be observed that the carbide particles gradually homogenize. After 9 h, the microstructure aged under long-term insulation, with coarse crystals and decreased toughness within the tissue. The improvement of low-temperature toughness is related to the replacement of ferrite pearlite microstructure with ferrite/spheroidized carbide microstructure. Spheroidization annealing reduces the stress concentration points inside the material by spheroidizing the carbides in the steel, forming a uniform spherical structure. This uniform microstructure can better withstand impact loads at low temperatures, typically exhibiting ductile dimples and fibrous features, indicating that the material undergoes plastic deformation before fracture.

The study on the effect of heat treatment on the fracture mechanism has revealed that the fracture mechanism of low-carbon steel exhibits brittle or ductile characteristics, which mainly depends on the relative ratio between the yield strength σs and the theoretical cleavage fracture strength σc. When the yield strength σs of the material exceeds the theoretical cleavage fracture strength σc, the fracture mechanism is mainly cleavage fracture; on the contrary, if the yield strength σs is lower than the theoretical cleavage fracture

strength σc, the material tends to undergo a plastic fracture process. Therefore, the influence mechanism of heat treatment on the impact toughness of Q235B is mainly attributed to the significant increase in yield strength σs caused by the improvement in the matrix during the heat treatment process.

As depicted in Figure 9, the Charpy V-notch impact energy (Kv) of Q235B steel at different temperatures after being held at 700 °C for 6 h is presented. Additionally, the impact energy data of ADI at various temperatures is measured and shown in Table 3. With the American standard ASTM as a reference, the low-temperature impact energy of carbon structural steel A36 at 0 °C is not less than 27 J [42]. The low-temperature impact energy performance of Q235B steel subjected to spheroidizing annealing treatment is far superior to its standard. The empirical formula is derived from the data in Table 3, with which the relationship between impact energy and temperature can be conveniently calculated. The empirical formula is as follows:

$$E = 328.8 + 1.817T - 0.01626T^2 \quad (1)$$

In the formula, E—impact energy and T—test temperature. Moreover, the coefficient of determination R^2 of this empirical formula is 0.992.

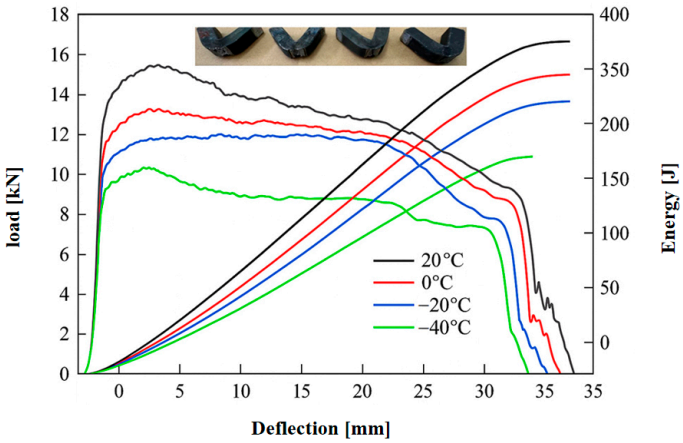

Figure 9. Dynamic load–displacement curve and absorption energy and post-impact macroscopic morphology diagrams.

Table 3. Impact energy of Q235B at different temperatures.

Temperatures [°C]	Average Energy [J]	Specimen 1	Specimen 2	Specimen 3
20	360.52	365.54	358.96	357.06
0	323.14	318.47	322.68	328.27
−20	291.62	295.71	292.03	287.12
−40	228.23	225.84	229.18	229.67

Under cryogenic conditions, the impact energy of Q235B steel significantly decreases with the reduction in temperature. At 20 °C, the specimen's average impact energy is 360.52 J, indicating that the material possesses high toughness and excellent energy absorption capability. At 0 °C, the impact energy drops to 323.14 J, a decrease of about 37.38 J compared to 20 °C, suggesting that the reduction in temperature has already begun to affect the steel's ductility. At −20 °C, the impact energy further declines to 291.62 J, which is approximately 31.52 J lower than at 0 °C. At −40 °C, the impact energy sharply falls to 228.23 J, a reduction of about 63.39 J from −20 °C, corresponding to an overall decrease of roughly 36.7%.

This trend indicates that as the temperature decreases, the material's overall capacity for plastic deformation is significantly weakened. From a mechanical standpoint, at low temperatures, limited atomic movement and dislocation activity facilitate the formation of stress concentrations within the material, which in turn promotes the early initiation and rapid propagation of cracks. Consequently, the specimen's ability to absorb impact energy is markedly reduced. The notable drop in energy—especially between −20 °C and −40 °C—suggests that the impact toughness of the material deteriorates in a non-linear fashion with decreasing temperature, highlighting the increasingly detrimental effect of low temperatures on the material's toughness. At low temperatures, due to the overall reduction in material ductility and the early formation and rapid propagation of cracks, the specimen's ability to absorb impact energy is greatly reduced. The presence of lamellar cementite in metallic materials increases the brittleness of the material, as it easily generates stress concentrations around it, thereby reducing the toughness of the material. The existence of lamellar cementite reduces the plastic deformation ability of the material, making it more prone to fracture when subjected to impact; thus, the low-temperature impact toughness of lamellar cementite is relatively poor. In contrast, spheroidal cementite has a more positive effect on the toughness of metallic materials. Spheroidal cementite can be better dispersed in the metallic matrix, reducing stress concentrations and thereby improving the toughness of the material. When used in a low-temperature environment, spheroidal cementite does not undergo brittle fracture because it can absorb more energy and reduce the propagation of cracks, thereby providing better low-temperature impact toughness. As shown in Figure 9, the absorption energy curves of all specimens are truncated before reaching a steady state. During the experiment, the macroscopic fracture morphologies of all specimens remain intact, indicating that the spheroidizing annealing treatment at 700 °C can improve the low-temperature impact toughness of the material. After 6 h of heat preservation treatment, Q235B steel exhibits excellent impact toughness.

At low temperatures, due to the reduced plastic deformation capability of the material, localized stress concentration effects become more pronounced. Lamellar cementite, due to its elongated morphology, forms sharp geometrical defects at the matrix interface, which readily induce local stress concentrations that favor crack initiation. This localized stress concentration diminishes the material's energy absorption capacity under impact loading, leading to a marked reduction in impact energy.

In this study, after Q235B steel was subjected to quenching + spheroidizing annealing treatment at 700 °C for 6 h, its impact toughness was significantly improved, with the room-temperature impact energy reaching 360.52 J and still remaining at 291.62 J at −20 °C. The mechanism lies in the fact that the spherical cementite reduces stress concentration, thereby achieving a balance between strength and toughness. However, the impact energy of ASTM A36 steel in Sujita's research was 158.33 J, which is much higher than this level [45].

Figure 10 presents the morphology of the impact fracture surface of the Q235B steel specimen within the temperature range of 20 °C to −40 °C. It can be observed from Figure 10 that as the temperature decreases, the brightness of the fracture surface gradually changes from dark to bright. At room temperature, the impact fracture surface contains numerous protrusions and depressions, with an uneven surface, resulting in an increased surface area and a darker brightness at the fracture. Additionally, a large number of dimples can be observed on the fracture surface; thus, the fracture exhibits obvious ductile fracture characteristics at room temperature. When the temperature is 0 °C, cleavage steps appear on the fracture surface, the number of dimples significantly decreases and becomes shallower, and cleavage planes and river patterns emerge.

When the temperature drops to −20 °C, the dimples at the fracture further decrease and become shallower, the cleavage planes and river patterns further increase, and the tearing edges decrease. At −40 °C, only a small number of dimples and tearing edges can be observed within the fracture, and the fracture morphology shows a large number of river patterns and uneven cleavage steps. Therefore, as the temperature decreases from 0 °C to −40 °C, the fracture exhibits both ductile and brittle fracture characteristics, belonging to a ductile–brittle mixed fracture. With the decrease in toughness, the impact toughness of Q235B steel decreases significantly; thus, the low-temperature impact toughness of Q235B steel is affected by temperature.

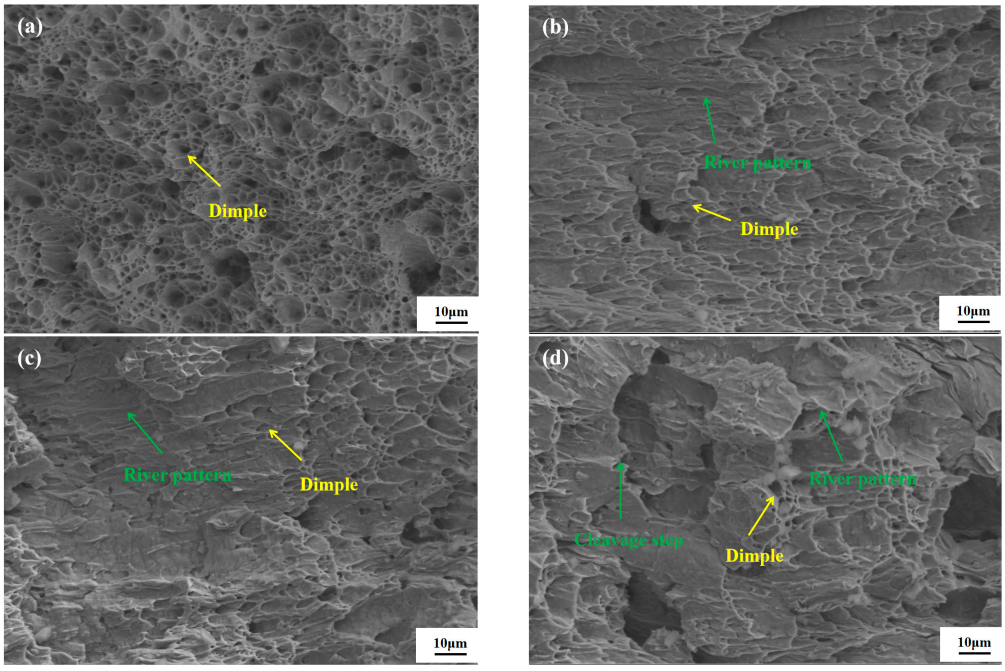

Figure 10. Impact fracture morphology of Q235B at different temperatures: (**a**) 20 °C; (**b**) 0 °C; (**c**) −20 °C; (**d**) −40 °C.

The ductile–brittle transition temperature can be evaluated through the Charpy impact test, which is the temperature corresponding to the equal area of the ductile and brittle regions on the fracture surface [46]. Based on the analysis of the fracture morphology, when the temperature drops to −20 °C, the river patterns occupy approximately half of the fracture surface, while the brittle fracture area accounts for approximately 50%. It can be inferred that the ductile–brittle transition temperature is approximately −20 °C. Therefore, when the experimental temperature is lower than the ductile–brittle transition temperature, the impact absorption energy will significantly decrease.

Based on Luo et al.'s [47] simulation analysis of impact tests at different temperatures, the yield strength changes at different temperatures are shown in the following Equation (1):

$$F_y = F'_y \exp[q_s(T' - T)] \quad (2)$$

In the formula:

F_y—represents the yield strength at temperature T;

F'_y—Yield strength at temperature T';

q_s—Q235B steel temperature sensitivity coefficient.

The theoretical cleavage fracture strength of Q235B hardly changes with temperature, so the effect of temperature on the fracture mechanism of low-carbon steel is caused by a significant increase in yield strength with decreasing temperature. This

means that under the strain rate and stress state corresponding to the standard Charpy impact test, the yield strength of Q235B steel after heat treatment near −20 °C is close to its theoretical cleavage fracture strength. Q235B steel exhibits a ductile-to-brittle transition temperature of approximately 0 °C [48]. Heat treatment can reduce the ductile–brittle transition temperature of Q235B. As the temperature drops below −20 °C, the yield strength of Q235B steel treated with spheroidization annealing increases, and the fracture mechanism transitions from ductile fracture to cleavage fracture.

4. Conclusions

The transformation of the microstructure of Q235 steel during spheroidization annealing reveals the following fact:

Through quenching spheroidization annealing treatment, the lamellar carbides in pearlite are transformed into spherical carbides through melting and spheroidization processes. The spheroidization process is usually accompanied by diffusion, where carbon atoms diffuse in the pearlite matrix and form dispersed spherical carbides during cooling. When the spheroidization annealing time is set to 6 h, the spheroidization uniformity reaches its optimum, the stress concentration effect is significantly reduced, and the ferrite structure has not yet grown, resulting in the best tissue uniformity. At this point, the tensile strength of the specimen reached 522 MPa, and the elongation rate was 31.28%. The spheroidization annealing process improves the toughness of the material.

Spheroidization annealing treatment reduces stress concentration points inside the material by spheroidizing the carbides in the steel, forming a uniform spherical structure and improving the low-temperature impact toughness of Q235B steel. After 6 h of insulation treatment, Q235B steel exhibits excellent impact toughness, with an impact energy of 295.71 J at −20 °C. Spheroidal annealing, resulting in a uniform microstructure, can better withstand impact loads at low temperatures and reduce the risk of brittle fracture. However, the continuous decrease in temperature will significantly reduce the impact absorption energy of Q235 steel.

The future research direction will focus on investigating the influence of spheroidizing temperature (650–750 °C) and cooling rate (air cooling/furnace cooling) on the morphology and distribution of cementite and establishing a quantitative prediction model for the process–microstructure–property relationship.

Author Contributions: Conceptualization, Y.L.; Formal analysis, X.L.; Funding acquisition, H.Z. and Y.L.; Investigation, X.L.; Methodology, H.Z.; Validation, G.L.; Writing–original draft, H.Z.; Writing–review and editing, G.L. All authors have read and agreed to the published version of the manuscript.

Funding: This research was financially supported by the National Key Research and Development Program of China (2022YFF0605300), the Technical Support Project of the State Administration for Market Regulation of China (2023YJ12), and the Key Laboratory of Special Machine and High Voltage Apparatus (Shenyang University of Technology), Ministry of Education (KFKT202106).

Data Availability Statement: The original contributions presented in this study are included in the article. Further inquiries can be directed to the corresponding author.

Conflicts of Interest: Author Hongkui Zhang was employed by the company Fushun CCTEG Inspection Center Co., Ltd. The remaining authors declare that the research was conducted in the absence of any commercial or financial relationships that could be construed as a potential conflict of interest.

Abbreviations

E	impact energy
T	test temperature
F_y	represents the yield strength at temperature T
F_y'	Yield strength at temperature T′
q_s	Q235B steel temperature sensitivity coefficient
CVN	Charpy V-Notch Toughness
SRO	Short-Range Ordering

References

1. Qamar, A.; Yao, H.X.; Muhammad, S.; Muhammad, R.; Sumbal, F. Metallic Minerals Production and Environmental Sustainability in China: Insights Using ARDL Bounds Testing and Wavelet Coherence Approaches. *Resour. Policy* **2024**, *92*, 105037. [CrossRef]
2. Fang, C.D.; Cheng, Z.H.; You, Z.; Chen, Z.H.; Peng, J.A. Detailed Examination of China's Clean Energy Mineral Consumption: Footprints, Trends, and Drivers. *Sustainability* **2023**, *15*, 16255. [CrossRef]
3. Kaźmierczak, U.; Górniak-Zimroz, Z. Accessibility of Selected Key Non-Metallic Mineral Deposits in the Environmental and Social Context in Poland. *Resources* **2021**, *10*, 6. [CrossRef]
4. Pan, R.K.; Cui, B.; Zhang, X.B.; Wang, Y.M.; Zheng, L.G. Study on Pressure Wave Response and Overpressure Attenuation Law of Explosion-Proof Doors. *Process Saf. Environ. Prot.* **2023**, *169*, 706–717. [CrossRef]
5. Kadam, S. Explosion-Proof DP Switch. *Process Plant Eng.* **2020**, *1*, 38.
6. Chen, J.X.; Chen, D.X.; Fan, Y. Design and Analysis of AGM Explosion Proof Plug Automatic Assembly and Inspection Production Line. *J. Phys. Conf. Ser.* **2024**, *2902*, 012002. [CrossRef]
7. Zhao, Z.C.; Ning, J.; Su, J.; Jiang, Q.W.; Liu, D.H.; Gao, Q.; Wang, A. Microstructure Characterization and Mechanical Behaviour of Laser Additive Manufactured Ultrahigh-Strength M54 Steel. *Mater. Res. Express* **2022**, *9*, 036506. [CrossRef]
8. Vinodh, S.; Ramakrishnan, T.; Padmanaban, R. Wear Behaviour of Friction Surfaced Al-Ni and Al-SiC Coatings over Mild Steel. *Mater. Res. Express* **2024**, *12*, 126507.
9. Liang, L.H.; Ren, Y.Y.; Tian, Y.; José, A.A.G.; Zhang, P.; Zhu, X.L. Role of Pseudomonas fluorescens FSYZ01 on the Corrosion Behavior of Q235B Carbon Steel in Oilfield Produced Water. *Environ. Sci. Pollut. Res. Int.* **2023**, *30*, 62590–62601. [CrossRef]
10. Wang, H.D.; Zhang, C.W.; Zhou, Z.Y.; Zhang, Y.Z.; Wang, K.S.; Wang, W.; Xu, X.L. Effect of the Microstructure on the Corrosion Behavior of Dissimilar Friction Stir-Welded 304 Austenitic Stainless Steel and Q235 Low-Carbon Steel Joints. *Mater. Res. Express* **2022**, *9*, 076508. [CrossRef]
11. Zuo, S.C.; Wang, D.C.; Yang, C.Q.; Hu, P.P.; Bi, R.; Du, B. Stress Relaxation Behavior of Low Carbon Steel at Different Temperatures. *Mater. Res. Express* **2023**, *10*, 105801. [CrossRef]
12. Zhang, C.J.; Wang, W.L. Study on Mechanical Performance of CoW/ZrO_2 Composite Film Prepared on Q235B Steel by Pulse Electrodeposition. *Int. J. Electrochem. Sci.* **2022**, *17*, 220424. [CrossRef]
13. Liu, X.Y.; Bu, Y.D.; Wang, Y.Q.; Guan, Y. Ultra-Low Cyclic Fatigue Fracture of Q235B and Q345B Steels and Their Butt Welded Joints. *Int. J. Steel Struct.* **2022**, *22*, 430–449. [CrossRef]
14. Tian, L.S.; Zhong, L.W.; Yan, P.B.; Chao, G. Study of Direct Alloying of Steels by Carbon Reduction of Cr_2O_3 under Vacuum. *J. Mater. Res. Technol.* **2024**, *28*, 3903–3910. [CrossRef]
15. Wang, X.J.; Sun, X.J.; Song, C.; Chen, H.; Han, W.; Pan, F. Enhancement of Yield Strength by Chromium/Nitrogen Alloying in High-Manganese Cryogenic Steel. *Mater. Sci. Eng. A* **2017**, *698*, 110–116. [CrossRef]
16. Dastur, Y.N.; Leslie, W.C. The Mechanism of Rapid Work Hardening in Hadfield Manganese Steel. *Strength Met. Alloys* **1979**, *1*, 619–623.
17. Saeed, A.A.; Mosecker, L.; Schwedt, A.; Bleck, W. Characterization and Prediction of Flow Behavior in High-Manganese Twinning Induced Plasticity Steels: Part I. Mechanism Maps and Work-Hardening Behavior. *Metall. Mater. Trans. A* **2011**, *43*, 1688–1704. [CrossRef]
18. Yu, Y.J.; Lan, L.F.; Ding, F.X.; Wang, L.P. Mechanical Properties of Hot-Rolled and Cold-Formed Steels after Exposure to Elevated Temperature: A Review. *Constr. Build. Mater.* **2019**, *213*, 360–376. [CrossRef]
19. Qiu, X.; Song, H.; Zhang, H.Z. Mechanical Properties of Hot-Stamped Spherical Shell Q235 Steel after Exposure to Elevated Temperature. *J. Mater. Civ. Eng.* **2024**, *36*, 04023537. [CrossRef]
20. Gurumurthy, B.M.; Sharma, S.; Kini, U.A.; Hegde, A.; Patil, A. Mechanical Characteristics Evaluation of Dual Phase and Related Hardening Techniques on AISI 4340 Steel. *J. Mech. Eng. Sci.* **2018**, *12*, 4018–4029. [CrossRef]
21. Htun, M.S.; Kyaw, S.T.; Lwin, K.T. Effect of Heat Treatment on Microstructures and Mechanical Properties of Spring Steel. *J. Met. Mater. Miner.* **2008**, *18*, 191–197.

22. Kini, U.A.; Sharma, S.S.; Nayak, S.Y.; Heckadka, S.S. Mechanical Characterization of Heat Treated EN 9 Steel. *Int. Conf. Eng. Inf. Technol.* **2017**, *17*, 18.
23. Hwang, H.; Bruno, G. Influence of the Initial Microstructure on the Spheroidization of SAE 52100 Bearing Steel. *Steel Res. Int.* **2015**, *87*, 112–125. [CrossRef]
24. Wu, H.Y.; Han, D.X.; Du, Y.; Gao, H.X.; Du, L.X. Effect of Initial Spheroidizing Microstructure after Quenching and Tempering on Wear and Contact Fatigue Properties of Gr15 Bearing Steel. *Mater. Today Commun.* **2022**, *30*, 103152. [CrossRef]
25. Dutta, S.; Panda, A.; Mitra, A.; Chatterjee, S.; Roy, R. Microstructural Evolution, Recovery and Recrystallization Kinetics of Isothermally Annealed Ultra Low Carbon Steel. *Mater. Res. Express* **2020**, *7*, 016554. [CrossRef]
26. Xu, Q.Z.; Liu, J.J.; Zhou, J.; Qiu, Z.H.; Yang, X.; Li, G. Surface Integrity, Corrosion Resistance, and Low-Temperature Impact Property of FH36 Marine Steel Subjected to Ultrasonic Surface Rolling Process. *J. Mater. Sci.* **2024**, *59*, 1736–1752. [CrossRef]
27. Du, Y.; Gao, X.H.; Wang, X.N.; Wu, H.Y.; Sun, C.; Sun, G.S.; Du, L.X. Low-Temperature Impact Fracture Behavior of Medium Manganese Steel with BCC-FCC Duplex Microstructures. *Metals* **2024**, *14*, 293. [CrossRef]
28. Gumuslu, T.; Kaba, M.; Atar, E.; Cimenoglu, H. Effect of Low-Temperature Nitriding on Impact-Sliding Wear Behavior of an Austenitic Stainless Steel at Room and Sub-Zero Temperatures. *Tribol. Int.* **2023**, *185*, 108560. [CrossRef]
29. Matthew, F.; Yusra, A.; Sreeramamurthy, A.A. Improving the Low-Temperature Toughness of a High-Strength, Low-Alloy Steel with a Lamellarization Heat Treatment. *Metals Mater. Int.* **2023**, *29*, 879–891.
30. *EN 10025-2:2019*; Hot Rolled Products of Structural Steels - Part 2: Technical Delivery Conditions for Non - Alloy Structural Steels. European Committee for Standardization: Brussels, Belgium, 2019.
31. Maleki, M.; Mirzadeh, H.; Zamani, M. Effect of Intercritical Annealing Time at Pearlite Dissolution Finish Temperature (Ac1f) on Mechanical Properties of Low-Carbon Dual-Phase Steel. *J. Mater. Eng. Perform.* **2019**, *28*, 2178–2183. [CrossRef]
32. Ghaemifar, S.; Mirzadeh, H. Enhanced Mechanical Properties of Dual-Phase Steel by Repetitive Intercritical Annealing. *Can. Metall. Q.* **2017**, *56*, 459–463. [CrossRef]
33. Maleki, M.; Mirzadeh, H.; Zamani, M. Influence of Intercritical Annealing on Microstructure and Mechanical Properties of Dual-Phase Steel. *Steel Res. Int.* **2018**, *89*, 1700412. [CrossRef]
34. Zhao, J.Z.; Wang, J.; Li, J.; Zhang, S.G.; Luo, F.H. The Effects of Super-Fast Heating Rate and Holding Time on the Microstructure and Properties of DP Fe-0.16C-1.4Mn Sheet Steel. *Materials* **2024**, *17*, 4982. [CrossRef] [PubMed]
35. Ohmura, T.; Tsuzaki, K. Evaluation of Matrix Strength of Fe-C As-Quenched and Quench-Tempered Martensite Using Nanoindentation Techniques. *J. Phys. IV* **2003**, *112*, 267–270. [CrossRef]
36. Tang, H.; Peng, J.X.; Peng, H.; Yang, Y.M.; Gao, Q.; Xiao, L.F.; Li, H.; Zheng, L.F.; Chen, Z.X.; Yang, Z.G. Test and Theoretical Investigations on Flexural Behavior of High-Performance H-Shaped Steel Beam with Local Corrosion in Pure Bending Zone. *Steel Res. Int.* **2024**, *315*, 118445. [CrossRef]
37. Maeda, M.; Shimamura, J.; Suzuki, S. Effect of Cementite Dispersion on Void Formation Process in Spheroidize-Annealed Steels. *ISIJ Int.* **2018**, *8*, 1490–1499. [CrossRef]
38. Najafi, M.; Mirzadeh, H.; Alibeyki, M. Tempering of Deformed and As-Quenched Martensite in Structural Steel. *J. Min. Metall. Sect. B Metall.* **2019**, *55*, 95–99. [CrossRef]
39. Ponge, D.; Raabe, D.; Song, R. Microstructure and Crystallographic Texture of an Ultrafine Grained C-Mn Steel and Their Evolution during Warm Deformation and Annealing. *Acta Mater.* **2005**, *53*, 845–858.
40. Nasiri, Z.; Mirzadeh, H. Spheroidization Heat Treatment and Intercritical Annealing of Low Carbon Steel. *J. Min. Metall. Sect. B Metall.* **2019**, *55*, 6. [CrossRef]
41. Pang, J.C.; Yang, W.F.; Wang, G.D.; Zheng, S.J.; Misra, R.D.K.; Yi, H.L. Divorced Eutectoid Transformation in High-Al Added Steels Due to Heterogeneous Nucleation of κ-Carbide. *Scr. Mater.* **2022**, *209*, 114395. [CrossRef]
42. *ASTM A36/A36M-05*; Standard Specification for Carbon Structural Steel Shapes, Sheets and Strip for Bridge Construction. ASTM International: West Conshohocken, PA, USA, 2005.
43. Qian, L.H.; Guo, P.H.; Zhang, F.C.; Meng, J.V.; Zhang, M. Abnormal Room Temperature Serrated Flow and Strain Rate Dependence of Critical Strain of a Fe–Mn–C Twin-Induced Plasticity Steel. *Mater. Sci. Eng. A* **2013**, *561*, 266–269. [CrossRef]
44. Rösler, J.; Harders, H.; Bäker, M. Mechanical Behavior of Engineering Materials. *Mater. Sci. Eng. A* **2007**, *458*, 1–11.
45. Sujita, S.S.; Sutanto, R.S. Study on Mechanical Properties of Pack Carburizing ASTM A36 Steel with Energizer Pomacea Canalikulata Lamarck Shell Powder. *Global J. Eng. Technol. Adv.* **2022**, *11*, 096–102. [CrossRef]
46. Sun, Y.F.; Hu, S.M.; Xiao, Z.Y.; You, S.S.; Zhao, J.Y.; Lv, Y. Effects of Nickel on Low-Temperature Impact Toughness and Corrosion Resistance of High-Ductility Ductile Iron. *Mater. Des.* **2012**, *41*, 37–42. [CrossRef]

47. Luo, Z.; Shi, Y.; Zhou, X.; Xue, X.; Peng, X. Low- and Elevated-Temperature Constitutive Model of Cold-Formed Titanium-Clad Bimetallic Steel Sections. *J. Constr. Steel Res.* **2024**, *221*, 108881. [CrossRef]
48. Liao, X.; Wei, H.; Feng, L.; Ban, H. Low-Cycle Fatigue Behavior for Stainless-Clad 304 + Q235B Bimetallic Steel. *Int. J. Fatigue* **2022**, *159*, 106831. [CrossRef]

Disclaimer/Publisher's Note: The statements, opinions and data contained in all publications are solely those of the individual author(s) and contributor(s) and not of MDPI and/or the editor(s). MDPI and/or the editor(s) disclaim responsibility for any injury to people or property resulting from any ideas, methods, instructions or products referred to in the content.